JSEE Vol. 21, No. 1, 2019 DOI:10.48303/jsee.2019.240803

Experimental and Numerical Investigation of Reverse Fault Rupture Interaction with Steel Frame Structures

Azadeh Salajegheh[1*], Mohammad Davoodi[2], Mohammad Kazem Jafari[3], and Meysam Fadaee[4]

1. Ph.D. Candidate, Geotechnical Engineering Research Center, International Institute of Earthquake Engineering and Seismology (IIEES), Tehran, Iran,
* Corresponding Author; email: a.salajegheh@iiees.ac.ir
2. Assistant Professor, Geotechnical Engineering Research Center, International Institute of Earthquake Engineering and Seismology (IIEES), Tehran, Iran
3. Professor, Geotechnical Engineering Research Center, International Institute of Earthquake Engineering and Seismology (IIEES), Tehran, Iran
4. Assistant Professor, Islamic Azad University, Science and Research Branch, Tehran, Iran

Received: 06/03/2017
Accepted: 06/01/2018

ABSTRACT

During large earthquakes, a soil deposit overlaying an active fault is suspected to experience quasi static differential settlement produced by propagation of bedrock fault rupturing. Such differential surface dislocations can cause severe damage to engineering framed structures. Although there is partly extensive literature in this field, in most previous studies, super structures are not considered in the analysis directly. This paper investigates the interaction of a frame structure located on top of a soil sediment with a reverse fault rupturing. For this purpose, a series of reduced scale 1 g box tests with a steel frame structure were conducted. Then, the same related numerical models were calibrated and validated using physical modeling results. To compare different structural system behavior against surface fault rupture, two types of steel framed structure including moment resisting frame and concentric braced moment resisting frame were selected in the numerical analysis. A brief sensitivity analysis on structure position relative to fault outcrop is performed using numerical Finite Element (F.E.) method for both types of structural systems. Different responses for sediment and structure are considered. The results show that deformation mechanism of structural elements in these two systems are basically different. Based upon the results of this research, the moment frame is suspected to have more severe structural damage or even complete destruction.

Keywords:
Reverse fault rupture; Fault rupture- soil-foundation- structure interaction; 1 g tests

1. Introduction

The past Turkey and Chi-Chi (1999) as well as Wenchuan (2008) earthquakes offered numerous examples of devastating effect of fault-rupturing to many structures like buildings, bridges, dams, roads and pipelines constructed on active faults. However, it was observed in some cases that in presence of a rigid and continuous foundation, the fault rupture may deviate from the structure or the differential displacement may change to rigid body rotation of structure without any considerable human losses. This can be evaluated as the interaction effect of surface fault rupture-soil-foundation-structure (FR-SFI) system. The phenomenon of fault rupture propagation through a soil layer and its interaction with foundation has extensively studied on the three categories: (a) study of case histories [1-2],

(b) physical modeling studies [3-6] and (c) numerical or analytical studies [7-11]. As a consequence, the foundation type and the superstructure loading play an important role in the response of structure and fault rupture propagation. It has been mentioned in previous studies [7, 10-12] that heavy structures supported on rigid mat or box-type foundations have better performance in comparison with those on single footings.

Despite relatively enough background literature in the field of modeling surface foundations on top of a soil layer subjected to fault rupture phenomena, there is not extensive research in the case of direct presence of structure. Anastasopoulos et al. [13] performed a short parametric study of typical 2 and 5-story residential structures subjected to normal fault dislocation. They studied coupled system response by changing parameters such as rigidity of the foundation, surcharge load of the superstructure, soil stiffness and the position of the structure relative to the fault rupture outcrop. Beam and column's cross sections are defined similar in all stories and have a linear behavior. No special detail is considered for connections. Despite the imprecise modeling of the structure, the results of this research can be used as an appropriate guidance. Hashemydahaj [14] considered the coupled effect of FR-SFSI for an aluminum small-scale structure (representing a present designed structure with soft story) and calibrated a numerical model based on the test results. Besides, the effect of changing the structure location is discussed using a brief numerical parametric study.

Considering shortcoming of literature, the effect of modeling of structure is investigated by both experimental and numerical models in the present study. The purpose is to develop a deeper insight into performance of different structural elements during fault rupture. This is done through studying a number of responses such as vertical surface profile of soil, structural drift ratio and relative rotation of elements and rigid body settlement of structure.

In order to study the response of FR-SFSI systems, a two-step procedure is used. The first step is to model free field fault rupture propagation and fault rupture-soil-foundation-structure system by 1 g reduced scale tests and calibration of numerical models using the result of these physical modelings. In the second stage, a parametric study is conducted to investigate the performance of two types of structural systems. In this study, a moment resisting steel frame and a concentric braced moment resisting steel frame are selected as different types of structural systems. The response of coupled system (FR-SFSI) is considered in a wide range of structure location on top of soil layer. The results demonstrate more acceptable performance of braced frame against reverse fault rupture phenomenon.

2. Physical Modeling

2.1. Model Geometry and Test Setup

The 1 g physical modeling approach is conducted in this research using the 1 g testing apparatus built in geotechnical laboratory of International Institute of Earthquake Engineering and Seismology (IIEES). The device is capable of modeling the normal and reverse faulting with different dip angles. The length and width of the split-box is 180 and 50 cm respectively and maximum soil depth of 60 cm, can be used in this device. The length of movable part (hanging wall) is 40 cm. In all tests, reverse fault rupture propagation with a dip angle of 45° is performed. The fault displacement is imposed at the base of the model at the rate of 2 mm per step in a quasi-static mode until the maximum value of 64 mm is reached. More details of this apparatus can be found in [6, 15-16].

2.2. Soil Sediment

The Firoozkooh sand (No. 161), a uniformly graded soil, is utilized for all experiments. Mechanical properties of soil are presented in Table (1) in which D_{50}, G_s, $(\gamma_d)_{\min}$, and $(\gamma_d)_{\max}$, are mean grain size, specific gravity, minimum and maximum dry density of soil respectively. To achieve soil layers with a uniform target relative density, the sand should be pluviated from a sand rainer with a specific height and velocity. The relative density of sand is selected to be approximately 80% that represents medium dense sand. The total alluvium height is 40 cm, which is poured in eight layers with 5 cm thickness. In order to allow visual inspection

Table 1. Mechanical properties of Firoozkooh sand.

Mechanical Properties of Soil			
D_{50} (mm)	G_s	$(\gamma_d)_{min}$ (gr/cm^3)	$(\gamma_d)_{max}$ (gr/cm^3)
0.25	2.61	1.42	1.71

of soil deformations, blue sand layers is placed in close proximity to the front face of apparatus.

To obtain peak and residual strength of sand, a series of direct shear tests are conducted in different normal stress levels, which represent 1 g test and prototype condition [6, 16]. For the reduced scale 1 g model tests, the normal stress is less than $\sigma_v < 10KPa$ that leads to increasing the sand peak friction angle into $\varphi_{peak} = 45^o$ [16, 17].

2.3. Structural Frame

The structure used for 1 g tests is a reduced-scale 2-story steel frame with one span at both longitudinal and transverse directions. Based on the dimensional limitation of the fault box, the scale factor of $N = 10$ is chosen for all physical models. The structure is designed according to conventional scaling relation in the 1 g field. The scaling factors for different parameters needed in the design have been obtained from Table (1) presented in [18]. The structure is made of two identical frames connected together with bolt connections. Beams and columns are loaded in gravity and seismic cases based on Code "ASCE7-05" and designed using allowable stress method of "AISC-ASD 01" and considering the scale rules. Design of structural elements based on (utilizing) these two codes, provides ability of considering the response of real-scale structures in the future researches. Columns and beams have box type cross section with 50×4 mm and 40×4 mm dimension respectively. All members are made of steel ST-37 with yield strength of $F_y = 2400$ Kg/cm^2 and bolts are type DIN-10.9 with ultimate strength of $F_u = 10000$ Kg/cm^2. Bolt type connection is selected to provide ability of assembling structural members for several times. This type of connection is also capable of modeling different level of connection rigidity by controlling the rate of bolt tightening. The different connection stiffness levels can be performed by this method. More structural details are shown in Figure (1).

At each story, there are three transverse beams that provide the stability of whole structure in out-of-plane direction. These tie beams are also heavier than other members and are used to impose gravity load on each story. Considering the width of fault box, the span length of structure in transverse direction is assumed to be 400 mm. The foundations are single footing type made of Plexiglas plates with 150×100 mm dimension and are bolted to base plates. The image of aforementioned structure is shown in Figure (2). A 3D view of structure is shown in Figure (2a). Beams, columns, transverse beams, base plates and connection plates are seen

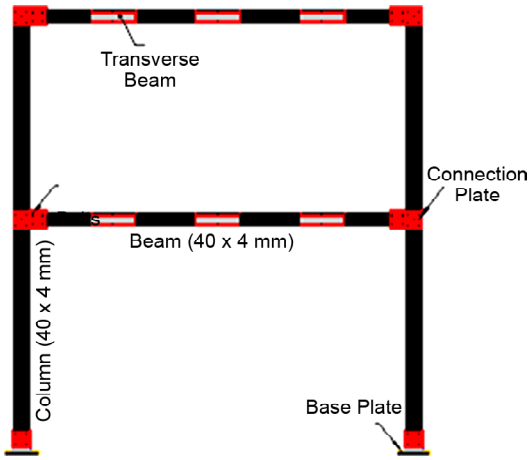

Figure 1. Schematic illustration of the structural frame.

(a)

(b)

(c)

Figure 2. (a) 3D view of assembled small scale structure, (b) closed view of beam to column connection, (c) closed view of column to base plate connection.

in this picture. The red strip markers are required for image processing technique to compute displacement and rotation of structural elements from consecutive photos. Details of beam to column and column to base plate connections are presented in Figures (2a) and (2b) respectively.

In this study, the ultimate bending moment capacity of connections is selected in such a way that beams and columns are capable of relative rotation. This can simulate some cases in which structural connections are not strong enough or soft story condition can be happen.

2.4. Model Instrumentation

In order to record test results, both image processing technique and digital instruments are used in the present study. Deformation created in alluvium, foundation and structural elements are inspected by digital image analysis using image processing software developed at IIEES [16, 19]. The software is upgraded and modified to considering presence of structure. To record structure displacement and rotation, red strips are pasted on beams and columns and traced constantly. Digital images of the deformed soil sample were captured through the Perspex front face at every 2 mm of imposed base dislocation, using a high-resolution (15 MP) canon digital camera. This set of the digital images are rectified according to derived optical parameters of the whole system. Then all output (displacement, rotation and strain fields) could be obtained by computing the optical flow between each pair of consecutive rectified images.

For more reliable measurement of produced displacements in different structural elements, a number of digital linearly variable differential transformers (LVDT) are positioned and named as shown in Figure (3). As shown in Figure (3), LVDT d11 and d16 with 200 mm amplitude are used for measurement of horizontal displacement of first and second story and d16 with 50 mm amplitude gives vertical displacement of the first story. Relative rotation of top corner angle at the second story is obtained by data from LVDT d12 and d14 (again with 50 mm amplitude). All data from LVDTs are recorded by a static multi point 100 channels data logger. In order to determine the magnitude of foundation rotation a digital rotation meter is positioned on left-back footing.

3. Calibration of Numerical Modeling

3.1. Simulation Method

Based on literature, the results of numerical analysis with F.E. method are in good agreement with field observation and physical modeling technique in case of fault rupture propagation (both in the free-field case and its interaction with foundation) [8, 13, 20]. To achieve such an agreement, essential requirement is to use a refined mesh and an appropriate nonlinear constitutive model for soil deposit [8, 21].

The problem is numerically simulated using the F.E. method and commercial F.E. code ABAQUS in this study. To calibrate numerical model and verify the effectiveness of proposed method, all numerical models are small scale. Due to the similarity of both structural frame and uniformity of fault rupture along out-of-plane direction, 2D plain

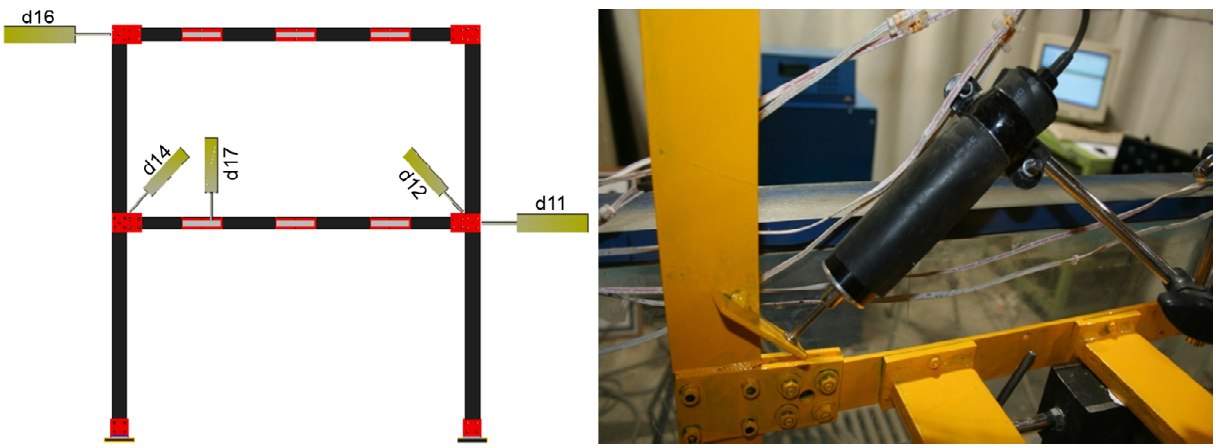

Figure 3. (a) Location and labeling of digital LVDTs; (b) Image of installed LVDT No. d12 with amplitude of 50 mm.

strain condition is used for the analyses. Although two-dimensional modeling has some shortcomings compared with 3D modelling, the results of our analysis show that 2D modeling leads to acceptable compatibility with the experiments. The soil medium is modeled with quadrilateral continuum elements and beams and columns are defined by 2-noded flexural elastic beam elements from steel. The boundaries of the model in the moving part are not fixed and both vertical and horizontal displacement can be applied on these boundaries. The displacements are applied with a quasi-static rate and in 5 mm steps in the Numerical models.

The beam-column and column-footing connections are modeled as plastic beam elements consisting of an elastic-perfectly plastic constitutive model. The foundation is modeled with linear elastic beam elements and is connected to soil using special contact elements. These contact elements are infinitely stiff in compression, follows Coulomb's friction law in shear (to model sliding). In order to model detachment of the foundation and its beneath soil, no resistance in tension is defined. The differential displacement representing base dislocation (base offset), is applied to left part of the model (hanging wall) in small consecutive steps.

Based upon the reasonable results of previous studies, a well-known constitutive model extensively used in QUAKER project [8, 13] is selected. This is an elasto-plastic constitutive model with Mohr-Coulomb failure criterion and isotropic strain softening is utilized in this paper. The model is applied in the finite-element code ABAQUS 2011 through a user subroutine. The most important parameters of soil in this constitutive model are E (Elastic Modulus of Soil), φ_{peak} and φ_{res} (peak and residual friction angle) and Ψ (dilation angle). These parameters can be calculated based on the direct shear test results of a soil sample [8]. The scale effects [22], is taken into account by an approximate simplified method which changes the limit value of plastic octahedral shear strain according to mesh size [8]. The value of peak friction angle has been determined in section 2-2. Considering all the above, the material parameters used for soil modeling are $E=120000$Kpa, $v=0.3$, $\varphi_{peak}=45°$, $\varphi_{res}=35°$, and $\Psi=13°$.

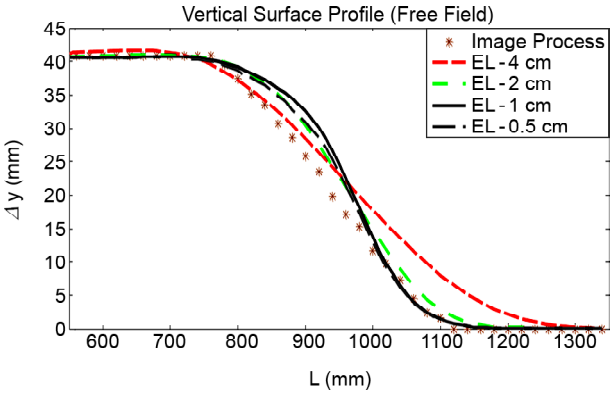

Figure 4. Comparison of free field vertical displacement profile obtained from image processing technique with F.E. method using different mesh size, for h= 40 mm.

3.2. Validation of Results

3.2.1. Results of Free Field Test

The results of numerical analysis for free field case are compared with the related 1 g experimental test. In order to achieve an optimum mesh size for soil medium, a series of analysis is conducted by different mesh size of 4.0, 2.0, 1.0 and 0.5 cm. The results are compared in terms of the vertical displacement profile of the ground surface for base offset of $h=40$ mm (Figure 4). According to Figure (4), both models with 1 cm and 0.5 cm mesh size, show good agreement with physical modeling (results of Image Processing Software). Because of lower analysis time and cost, the model with 1 cm mesh size is selected for all numerical modeling in this study. The location of fault emergence at the ground surface, the rupture path and the value of displacement at soil surface, are well predicted in the analysis. The fault outcrop on soil surface is located at $x=780$ mm from the left side of apparatus box.

The observed discrepancies in the surface profile gradient are associated to some factors such as very low confining pressures in small scale 1 g tests, relatively simplified constitutive model used for the analyses and side effect of Plexiglas plates.

3.2.2. Fault Rupture-Soil-Foundation-Structure Interaction

After modeling the free-field case, the effect of presence of a structure on top of an outcropping fault is investigated by both physical and numerical methods. For this purpose, the results of two 1 g tests are discussed in this paper. The position of structure

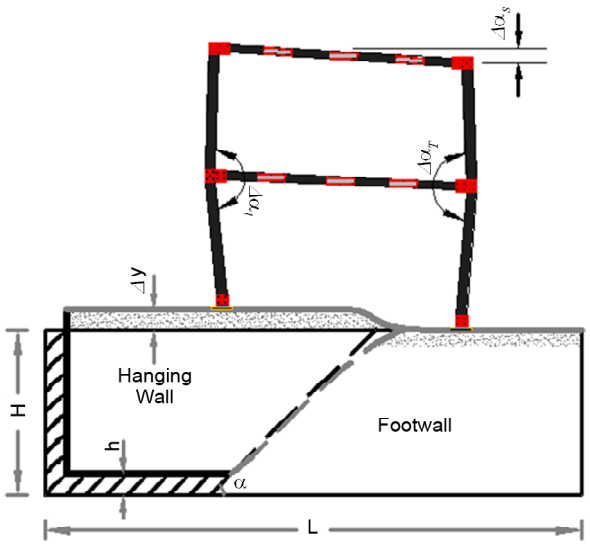

Figure 5. Problem definition and engineering interested variables studied herein.

is the only parameter changed in these two tests. The problem definition and its variables are depicted in Figure (5). All structural details are as mentioned in section 2-3. Soil layer is considered the same as free field test.

3.2.2.1. Results of Test #1

The first test is named as "SFSI-04-H400-X500" and the distance between left column and left side of fault rupture apparatus is X=500 mm that cause the free field fault outcrop, approximately in the middle of structure span. The connection stiffness (plastic moment capacity) of left and right columns is equal at both stories.

The rectified image for general deformed shape of soil and structure with superimposed shear strain contours of alluvium, is compared with numerical deformed mesh (Figures 6a and 6b). The comparison between general deformed shape of whole system and plastic shear strain contours reveals satisfactory agreement. The right column located on footwall shows more relative rotation of elements in contrast with left column (on hanging wall). Moreover, vertical displacement profile of soil surface is compared with physical observation (Figure 6c).

To verify the result of numerical modeling for structural part, the magnitude of point displacement at position of LVDT d11 and d16 (at first and second story respectively) is depicted in Figure (7). The response of physical modeling is obtained from both digital instrumentation and image processing

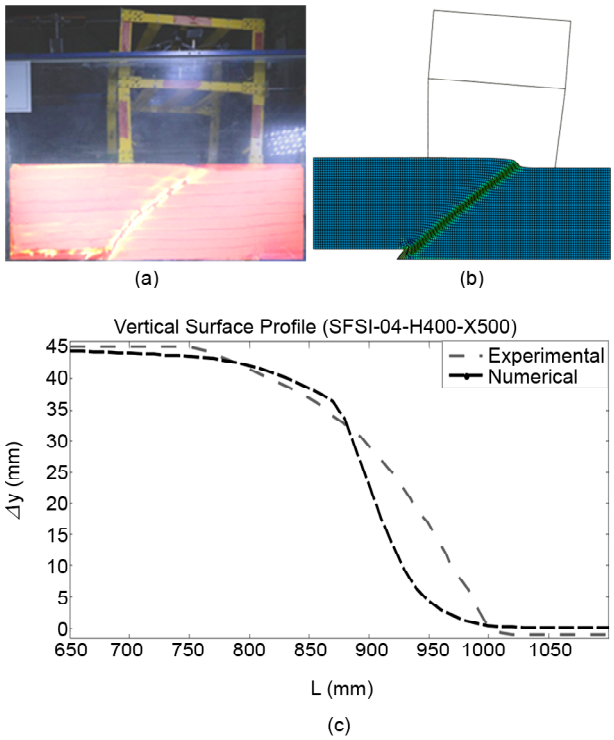

Figure 6. Interaction of reverse fault rupture and steel frame structure positioned at X=500 mm (SFSI-04-H400-X500); comparison of experimental with numerical analysis results for bedrock fault offset h=45 mm: (a) photo of the deformed model with superimposed plastic shear strain vectors computed through image analysis, compared with F.E. deformed mesh, (b) vertical displacement surface profiles of soil obtained image processing compared with F.E. analysis results.

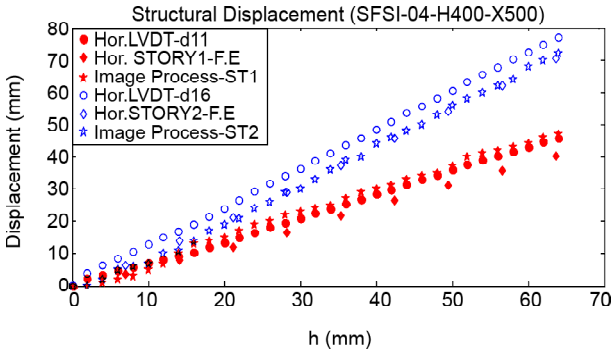

Figure 7. Test "SFSI-04-H400-X500": horizontal displacement of structural points as a function of bedrock offset h; comparison of results from digital LVDTs, image processing method and numerical F.E. analysis at position of LVDT d11 and d16 (the first and the second story).

method. Comparison of 1 g test and F.E. method in terms of structural displacement shows reasonable adjustment between responses.

3.2.2.2. Results of Test #2

In the second test named as "SFSI-02-H400-X250", the structure is located at X=250 mm that means that free-field fault outcrop, is approximately

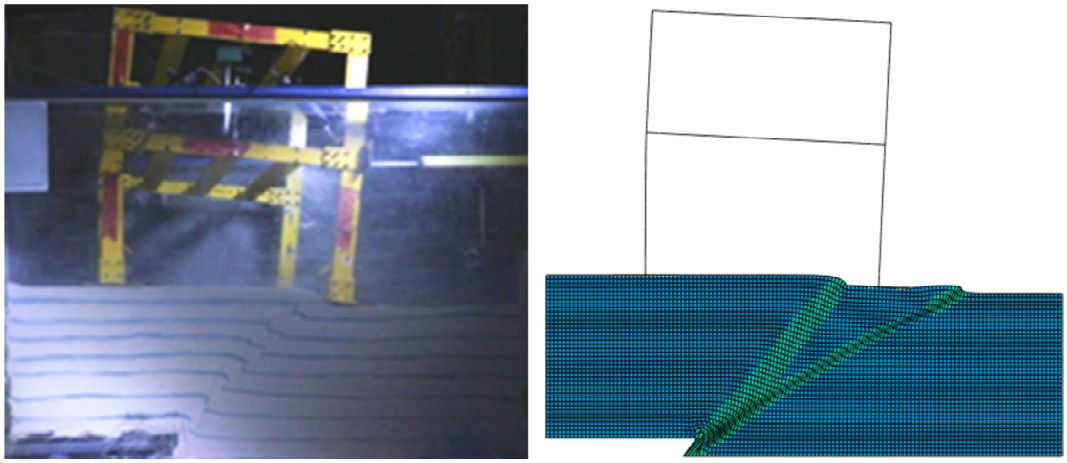

(a) (b)

Figure 8. Interaction of reverse fault rupture and steel frame structure with single footing, positioned at X=250 mm (SFSI-02-H400-X250); comparison of experimental with numerical analysis results for bedrock fault offset h = 45 mm: (a) rectified photo of the deformed model produced with image processing software (b) deformed mesh of structure plus plastic shear strain contours from numerical model.

near the right column of structure. Similar to test #1, the rectified image of deformed shape of whole model shows a qualitative similarity with finite element method (Figure 8). In this case the relative rotation is considered at left column but the right column mainly tolerates rigid body rotation. This is different with result of previous case in which the right column has experienced more relative rotation. The main reason is because of changing the relative location of imposed fault rupture and structure. The fault rupture is outcropped just before the right corner of right foundation and not continued to its left corner. However, this could not prevent rotation and separation of foundation from soil.

Again, verification of structural performance is carried out by comparing point displacements at position of LVDTs d11 and d16 (Figure 9). There are

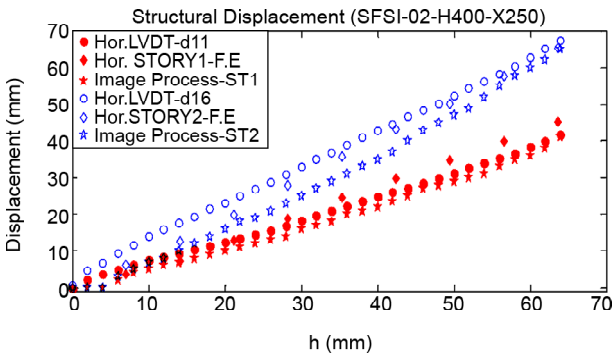

Figure 9. Test "SFSI-02-H400-X250": horizontal displacement of structural points as a function of bedrock offset h; comparison of results from digital LVDTs, image processing method and numerical F.E. analysis at position of LVDT d11 and d16 (the first and the second story).

acceptable differences (almost 12% in first story and 2.5% in second story at higher levels of base offset) between results of numerical and physical modeling at both stories. This implies that the developed numerical model could be used with a reasonable certainty. The difference between results of LVDTs and image processing technique is somewhat more significant (almost 8% in first story and 10% in second story at higher levels of base offset) and refers to inherent errors of this method such as lighting volume, calibration error and low transparency of Plexiglas plate.

4. Results of Parametric Numerical Study

Having validated the F.E. method using ABAQUS software, a numerical parametric study is conducted to investigate the effect of structural system and its location on performance of structure. In this study, two types of structural system are selected. The first type is a moment resisting steel frame, which is named as system "TYPE-A" here after. The second one is a dual system named as "TYPE-B" and is a moment resisting concentric braced steel frame. A series of analyses is performed by changing structure location for both the above-mentioned TYPE-A and TYPE-B systems. The structural characteristics of system TYPE-A, is exactly similar to verified finite element model of previous section. In system TYPE-B, X-shape concentric bracing are added to moment resisting frame, in both stories. The cross section of bracings is selected

to be 30×4 mm that is in accordance with dimension of beams and columns' cross section. As is common in construction, bracing connections are modeled to be hinge type. In comparison with the previous models of section 3, the length of soil layer is changed in all analyses of this section. The model length is selected to be 220 cm to achieve a wide range of structure position. A number of analyses among the 15 locations (X=35 cm up to X=130 cm) are performed. The results for both types of structural systems are presented in the following.

4.1. Moment Frame Results

For TYPE-A structure, four different deformation mechanisms in soil layer and structure are observed which are depicted in Figure (10) and can be classified as the below:

A-1) In the case of ($35 \leq X < 45$) both columns are located on hanging wall, although the outcrop of fault rupture is just located beneath the right footing. Due to the footing stiffness and weight, the width of fault outcrop is more than free field case and a little surface inclination could be seen beneath the right column. However, drift and rotation of both columns are in a same range and structure undertakes rigid body rotation (Figure 10a).

A-2) In the case of ($45 \leq X < 70$), the fault outcrop is steeper and the differential displacement between left and right footings is greater in comparison with case-1. Like the previous case, the structure tolerates more rigid body rotation instead of relative rotation of elements. However, the values of drift and total settlement of structure is greater in this location (Figure 10b).

A-3) In the case of ($70 \leq X < 90$), the left column is located on hanging wall and will move upward during fault rupturing while right column is on foot wall and does not move vertically at base. This differential displacement at structure base leads to the rotation of beam relative to column, especially in the first story. The magnitude of drifts and relative rotation in the right column is significantly larger than the left column. The vertical ground surface profile is similar to the free-field case with a steep outcrop located between two axes of structure. In this case, surface outcrop does not impact on any of footing (Figure 10c).

A-4) In the case of ($90 \leq X \leq 120$), the rupture outcrop is observed under the left footing. The relative rotation of right column is more considerable and much more than case-3. Figure (10d) shows that the deformation mechanism in case-4 is the most devastating scenario. Some disturbance is seen in surface profile beneath the left footing, in comparison with the free-field case. Higher values of X ($X > 110$), less values of relative rotation and drifts in both columns are seen.

4.2. Braced Moment Frame Results

In system TYPE-B, the issue is somewhat different. In all locations, the structure experience rigid body rotation but no relative rotation of elements

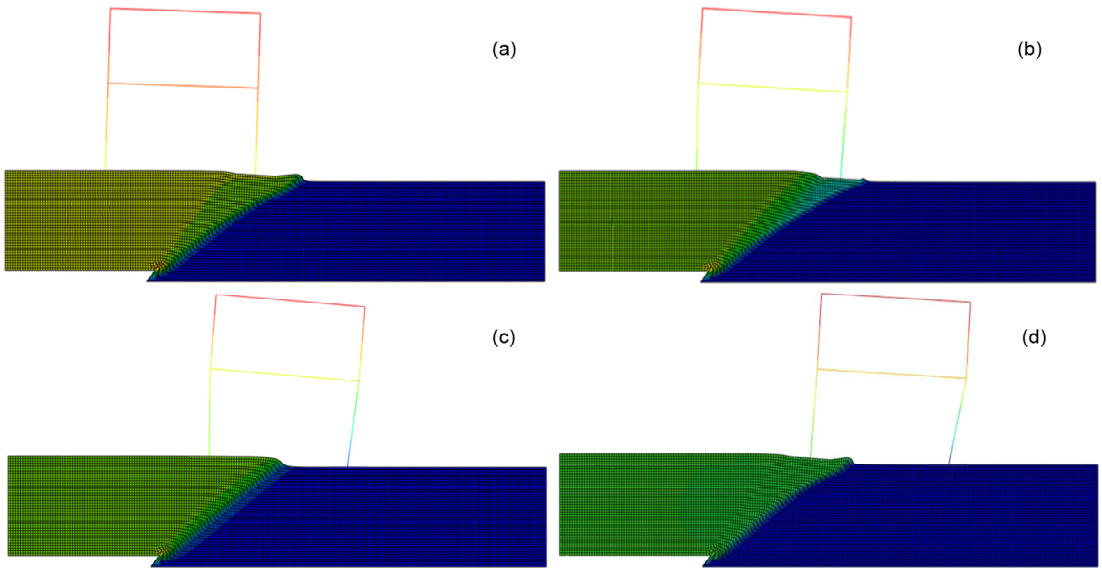

Figure 10. The effect of structure location on deformation mechanism of structure TYPE-A and soil deposit; Deformed mesh with displacement contours for bedrock fault offset h = 45 mm (a) X = 400 mm (b) X = 550 mm (c) X = 80 mm (d) X = 1000 mm.

is observed. In this case, the whole structure has a more geometric stiffness due to the existence of brace elements and behaves similar to a space truss. This prevents structural elements from relative rotation. Thus in all locations, the deformation mechanism of structure is the same but the maximum value of displacements varies considerably. In system TYPE-B according to the soil surface profile and structural displacements, four main mechanisms can be seen as below (Figure 11):

B-1) In the case of ($30 \leq X < 60$) the fault outcrop is located nearby the right footing and push the right column. This produce a tensile force in brace connected to left footing and causes uplift. The separation between left foundation and its beneath soil is depicted in close view of Figure (11a). In some locations ($X = 50$ and 55), the right footing is separated from the soil in a small part of its right side.

B-2) In the case of ($60 \leq X < 70$) the fault outcrop is located just before the left corner of right footing, but soil beneath the foundation is affected by fault rupture and a separation between soil and footing is considered in middle part of right footing (sagging deformation). This can be seen in close view of Figure (11b). Similar to "Case-1", the left foundation separates from soil due to uplift forces produced by brace elements (Figure 11b).

B-3) In the case of ($70 \leq X < 100$) the fault outcrop is located between two columns (almost middle of structure span) and soil surface profile is not so affected by presence of structure. Therefore, vertical ground surface profile is similar to the free field case. Such as "Case-3" in structure TYPE-A, the left and the right columns are located on hanging wall and foot wall respectively, which leads to a differential base displacement between the two columns. These differential settlements cannot produce relative rotation in connections and change to rigid rotation of whole structure (Figure 11c).

B-4) In the case of ($100 \leq X < 120$) the fault outcrop is located beneath left columns, but differential displacement between hanging and foot wall are changed into two more smooth step instead of a steep outcrop in this location. Therefore, the value of differential base displacement and following rigid body rotation of structure will decrease (Figure 11d). It should be noted that when $X \leq 120$, both columns are located on foot wall and structure almost is not affected by fault rupture.

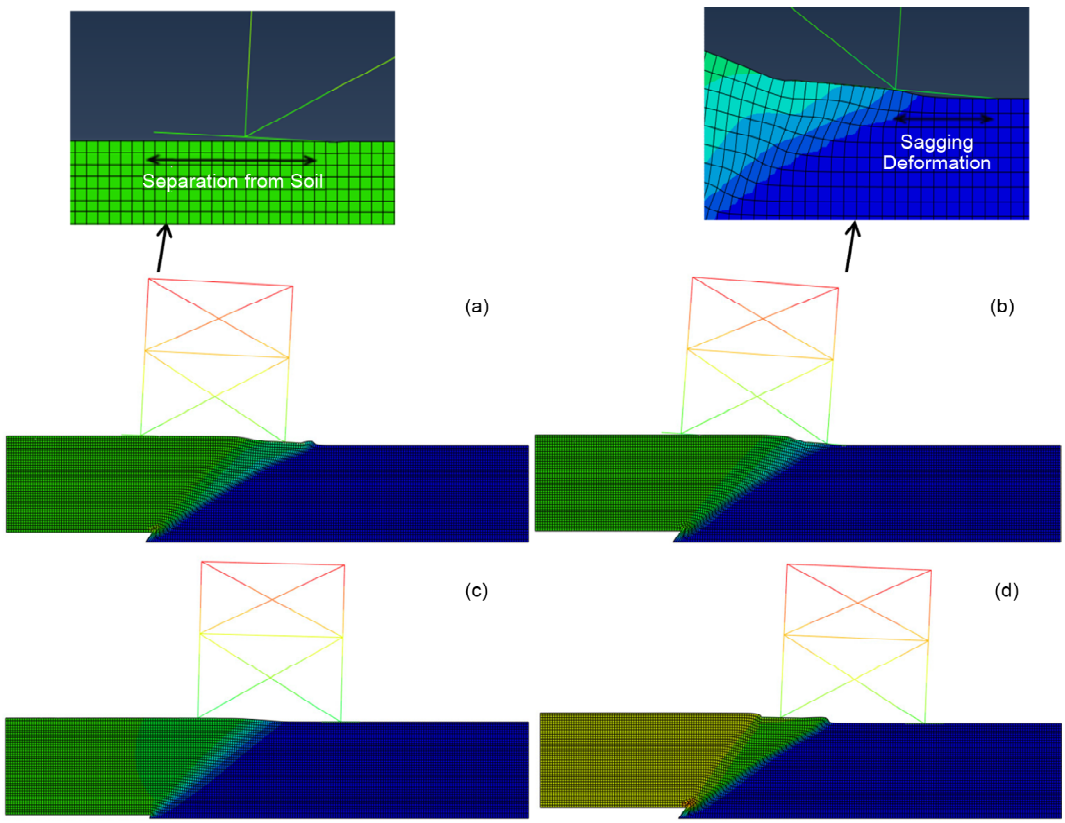

Figure 11. The effect of structure location on deformation mechanism of structure TYPE-B and soil deposit; Deformed mesh with displacement contours for bedrock fault offset h = 45 mm (a) X = 550 mm (b) X = 600 mm (c) X = 700 mm (d) X = 1000 mm.

4.3. Results and Discussion

Considering the above mechanisms and in order to ease of study, for each type of structure the results of only four locations (which are the best representative for all locations of structure in that mechanism) are presented. For system TYPE-A, these locations are X=40, 55, 80 and 100 cm while for structure TYPE-B, the most critical locations are X= 55, 60, 70 and 100 cm. However, the difference between results of X= 70, 75 and 80 cm is negligible for braced structure. Therefore, to compare the results for both structural systems, the locations X=40, 55, 60, 80 and 100 are selected. The response of soil deposit and structure are discussed in the following in terms of parameters such as vertical surface of soil, drift ratio, vertical settlement of structure and relative rotation of elements.

The vertical ground surface profile for four representative locations of structure "TYPE-A" as well as the free-field case are shown in Figure (12). As mentioned before, when structure is located at X=80 cm, the surface profile has the most similarity to the free-field case. At other structure positions, some affected sloped area is observed due to the presence of foundation and bifurcation of fault rupture. Surface profile at X=40 and X=100 cm are the same. Despite fault outcrop is beneath the right and left footing for X=40 and 100 cm respectively, symmetry of structure leads to a similar surface profile.

Figure (13) shows the variation of drift ratio parameter for right and left column at the first story

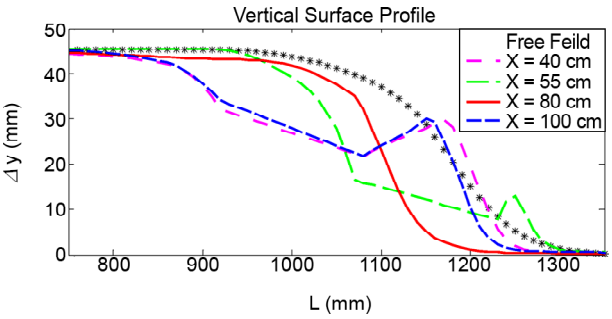

Figure 12. The effect of structure position on vertical surface profile of soil for bedrock fault offset h=45 mm.

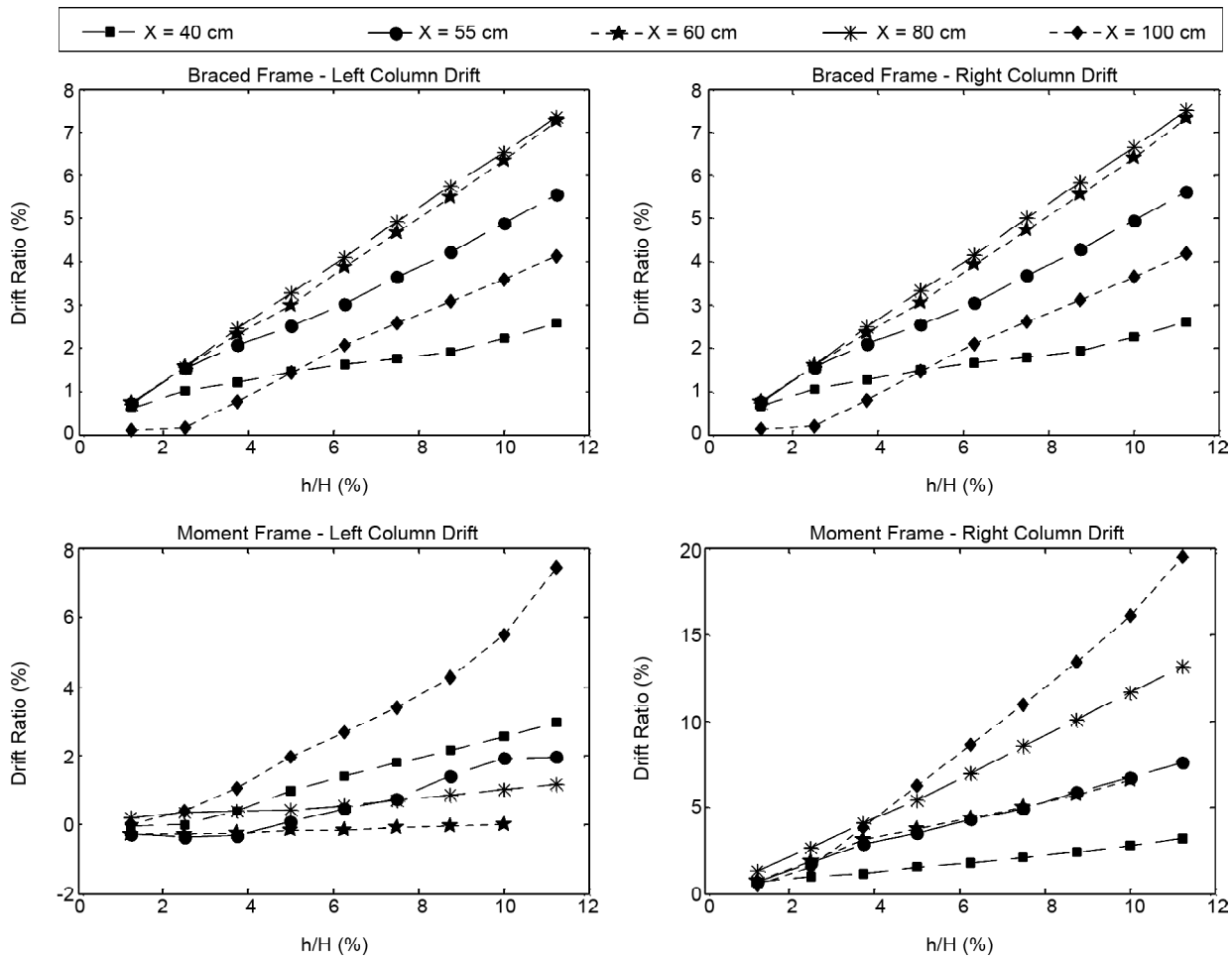

Figure 13. The effect of structure position on Drift ratio of first story columns for both system TYPE-A and TYPE-B.

for all different locations and both structural systems. For right column of system "TYPE-A", the more distance from left part of model (X), the larger value of drift ratio. This is not true for the left column. This column experiences the most drift ratio for case X=100 and X=40 cm respectively while the minimum value of drift ratio are produced when X=60 and X=80 cm. As mentioned before, the most critical scenario happens when X=100 cm (mechanism-4). The maximum value of drift ratio for right and left column is equal by 19.5% and 7.42% respectively. Such a large magnitude of drift ratio exceed much more than allowance values and can lead to serious damage and even overturning and/or destruction of structure.

In system "TYPE-B", the displacement pattern for both columns is the same. Drift ratio graphs show almost equal values for left and right columns, which is related to rigid rotation of braced frames. The maximum value are observed for X=80 and X=60 cm (7.51% and 7.33%) respectively. Besides, drift ratios in braced frame are considerably smaller than moment frame that can improve the performance of structure against fault rupture phenomenon.

The relative rotation percent of both left and right columns in all location of both structural systems are illustrated in Figure (14). The relative rotation of columns has been calculated based on the trigonometric equations. Each angle at each story is obtained by the general equation $\theta = \cos^{-1}(\frac{L_1^2 + L_2^2 - L_3^2}{2.L_1.L_2})$ in which L_1 and L_2 are the adjacent sides and L_3 is the opposite side of angle (say θ). Calculating all angles at both stories, the relative rotation of columns can be obtained summing the value of related angles. When the structure deforms during surface fault rupture, the angle between two columns of the first and the second stories changes from its initial value of 180°. These new angles are called $\Delta\alpha_1$ and $\Delta\alpha_r$ for left and right columns respectively and are depicted in Figure (5). The relative rotation angle is obtained by reducing $\Delta\alpha_1$ and $\Delta\alpha_r$ from 180°. In order to compare a normalized parameter, results are presented in terms of relative rotation percent (R.R.P.). The value of this parameter for the left and the right columns is obtained using equations $(R.R.P)_1 = ((180-\Delta\alpha_1)/180 \times 180$ and $(R.R.P)_r = ((180-\Delta\alpha_r)/180 \times 180$.

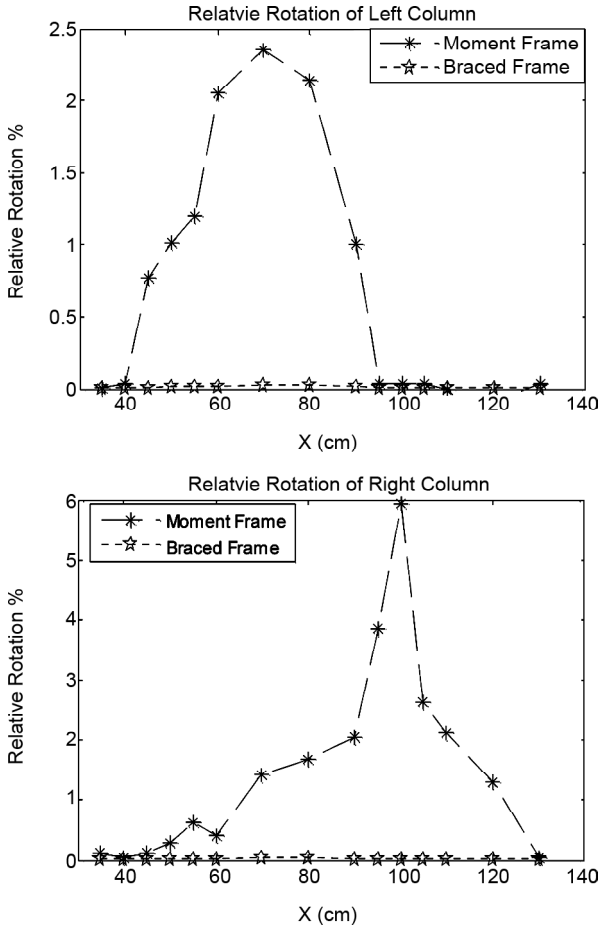

Figure 14. Columns relative rotation percent for both system TYPE-A and TYPE-B, as a function of structure location for base offset h/H = 11.25% (h = 45 mm).

Figure (14) proves that the brace elements almost prevent any relative inclination in structural members. Moment frame structure shows a large number of relative rotation in both columns, in while there are more values of this parameter in the right column. For both columns, the results follow a same trend but are different in value and location of producing maximum response.

According to Figure (14), the maximum value of $(R.R.P)_r$ is seen in location X=100 cm. This confirms the results of four classified mechanism of moment frame deformation that illustrated the more critical case occurred in location X=100 cm. It is obvious that such a high range of relative rotation in elements can lead to the destruction of connections and finally devastating damage on whole structure.

Another displacement response that is considered here, is the rigid vertical settlement of structure versus its location (Figure 15). This parameter is

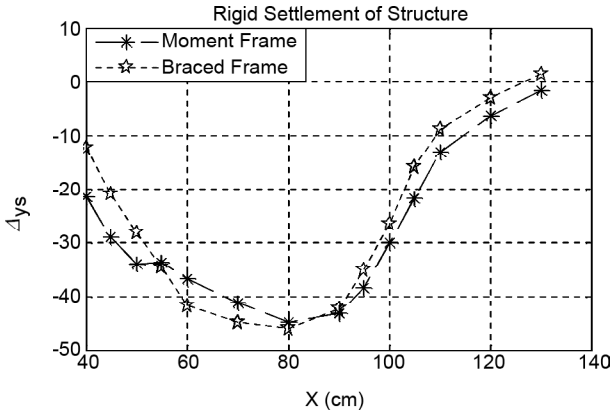

Figure 15. Rigid settlement of structure for both system TYPE-A and TYPE-B, as a function of structure location for base offset h / H=11.25% (h = 45 mm).

represented by Δy_s and depicted in Figure (5). For moment frame system, the maximum value is related to case X= 80 cm and is equal to 47.1 mm. In contrast with drift ratio response, the position X= 100 cm is not the worst case because the maximum differential base displacement is occurred when X= 80 cm (this can be seen through soil surface profile in Figures (10) and (12). For braced frame, the maximum rigid settlement values is observed when 70 ≤ X ≤ 90. Besides, for both types of structural systems, the rigid settlements has not considerable difference in magnitude and general trend of variation.

5. Conclusions

In the present study, the interaction effect of reverse surface fault rupture propagated through a soil deposit and two types of steel frame structures with single footings is investigated. Numerical analysis with finite element method shows appropriate agreement with physical 1 g modeling which indicates the effectiveness of numerical modeling assumption. Based on validated finite element, a brief parametric study on structure location - changing position from left side of hanging wall to right side of foot wall- is conducted. The main results of these analyses could be summarized as below:

- The general deformed shape of soil deposit and structure in numerical analysis shows an adequate conformity with 1 g test results. Of course, some incoherence between these two methods is observed. In the second test in which X=250 mm, the fault rupture outcrop is stopped just before the left footing. However, plastic shear strain contours in the F.E. model show diversion of fault rupture into two branches. The main branch is stopped before the left corner of foundation and the second path is propagated to its right corner.
- The soil surface profile is more affected when the fault rupture path is located near or beneath each of foundations. It seems that the stiffness of footing and weight of structure leads to some discrepancies in strain field and cause the deviation of fault rupture near the foundations.
- In the moment frame structure, high values of relative rotation, drift ratio and rigid body rotation are observed, which can lead to severe damage of structure. The most critical deformation mechanism is observed when the fault rupture outcrop impacts the right footing. Generally, it can be concluded that some kind of protective system is needed for moment frame structures subjected to surface fault rupture.
- The main trend of structural performance for braced moment frame system is basically different with the just moment frame system. The braced frame shows just rigid rotation without considerable relative rotation in structural members. Due to the tensile force in brace elements, the separation of foundation from its beneath soil is observed in some cases. It can be said that the existence of brace elements has improved the overall performance of structure against surface fault rupturing.
- Drift ratio in both structural systems exceed allowable serviceability limit in most location but the values are much smaller in braced frame. The most critical location is not necessarily when fault outcrop in beneath each of foundations. The observed displacement trend in the moment frame structure has a more critical condition because the drift ratio in left and right columns is not equal in this structural system.
- The results of this research reveal that moment frame structures almost have an out-of-service condition or experience high level of damage. It is not reliable to construct this kind of structure with single footing in areas suspected to surface fault rupture. Adding brace elements to frame can reduce the risk of structural damage and improve

the performance of whole system. Finally, it should be noted that results of this paper are related to a limited number of physical and numerical modeling. For more comprehensive conclusions, more extensive study on real scale numerical models should be performed.

Acknowledgment

The authors would like to acknowledge the technical and financial support of IIEES under the research project "Investigation of the Coupling Effect of Reverse Fault Rupture-Soil-Foundation-Framed Structure", (CODE- 598) and also express their gratitude to the members of geotechnical and structural laboratories.

References

1. Anastasopoulos, I. and Gazetas, G. (2007) Foundation-structure systems over a rupturing normal fault: Part I. Observations after the Kocaeli 1999 earthquake. *Bulletin of Earthquake Engineering*, **5**(3), 253-275.

2. Faccioli, E., Anastasopoulos, I., Gazetas, G., Callerio, A., and Paolucci, R. (2008) Fault rupture-foundation interaction: selected case histories. Bulletin of Earthquake Engineering, **6**(4), 557-583.

3. Bransby, M., Davies, M.C., El Nahas, A., and Nagaoka, S. (2008) Centrifuge modelling of reverse fault-foundation interaction. *Bulletin of Earthquake Engineering*, **6**(4), 607-628.

4. Bransby, M., Davies, M.C., and Nahas, A.E. (2008) Centrifuge modelling of normal fault-foundation interaction. *Bulletin of Earthquake Engineering*, **6**(4), 585-605.

5. Ahmed, W. and Bransby, M.F. (2009) Interaction of shallow foundations with reverse faults. *Journal of Geotechnical and Geoenvironmental Engineering*, **135**(7), 914-924.

6. Moosavi, S., Jafari, M., Kamalian, M., and Shafiee, A. (2010) Experimental investigation of reverse fault rupture-rigid shallow foundation interaction. *International Journal of Civil Engineering*, **8**(2), 85-98.

7. Anastasopoulos, I. and Gazetas, G. (2007) Foundation-structure systems over a rupturing normal fault: Part Ii. Analysis of the Kocaeli case histories. *Bulletin of Earthquake Engineering*, **5**(3), 277-301.

8. Anastasopoulos, I., Gazetas, G., Bransby, M., Davies, M., and El Nahas, A. (2007) Fault rupture propagation through sand: Finite-element analysis and validation through centrifuge experiments. *Journal of Geotechnical and Geoenvironmental Engineering*, **133**(8), 943-958.

9. Loukidis, D., Bouckovalas, G.D., and Papadimitriou, A.G. (2009) Analysis of fault rupture propagation through uniform soil cover. *Soil Dynamics and Earthquake Engineering*, **29**(11), 1389-1404.

10. Tolga Yilmaz, M. and Paolucci, R. (2007) Earthquake fault rupture-shallow foundation interaction in undrained soils: A simplified analytical approach. *Earthquake Engineering and Structural Dynamics*, **36**(1), 101-118.

11. Paolucci, R. and Yilmaz, M. (2008) Simplified theoretical approaches to earthquake fault rupture-shallow foundation interaction. *Bulletin of Earthquake Engineering*, **6**(4), 629-644.

12. Gazetas, G., Pecker, A., Faccioli, E., Paolucci, R., and Anastasopoulos, I. (2008) Preliminary design recommendations for dip-slip fault-foundation interaction. *Bulletin of Earthquake Engineering*, **6**(4), 677-687.

13. Anastasopoulos, I., Callerio, A., Bransby, M., Davies, M.C., Nahas, A.E., Faccioli, E., Gazetas, G., Masella, A., Paolucci, R., and Pecker, A. (2008) Numerical analyses of fault-foundation interaction. *Bulletin of Earthquake Engineering*, **6**(4), 645-675.

14. Hashemydahaj, S.K. (2012) *3D Experimental and Numerical Analysis of Fault Rupture-Soil-Foundation-Structure Interaction*. M.Sc. Thesis, National Technical University of Athens, School of Civil Engineering.

15. Moosavi, S. (2010) *Earthquake Fault Rupture Propagation through Soil, Reduction of Seismic Risk through the Application of*

Geotechnical Engineering Techniques. Ph.D. Thesis, International Institute of Seismology and Earthquake Engineering.

16. Fadaee, M., Anastasopoulos, I., Gazetas, G., Jafari, M., and Kamalian, M. (2013) Soil bentonite wall protects foundation from thrust faulting: Analyses and experiment. *Earthquake Engineering and Engineering Vibration*, **12**(3), 473-486.

17. Lade, P.V., Cole Jr., D.A., and Cummings, D. (1984) Multiple failure surfaces over dip-slip faults. *Journal of Geotechnical Engineering*, **110**(5), 616-627.

18. Fadaee, M., Jafari, M.K., Kamalian, M., and Mustafa, S.A. (2012) Fault rupture propagation in alluvium and its interaction with foundation: New insights from 1 g modelling via high resolution optical image processing techniques. *Journal of Seismology and Earthquake Engineering*, **14**(4), 271.

19. Anastasopoulos, I., Gazetas, G., Bransby, M., Davies, M., and El Nahas, A. (2009) Normal fault rupture interaction with strip foundations. *Journal of Geotechnical and Geoenvironmental Engineering*, **135**(3), 359-370.

20. Bray, J.D., Seed, R.B., Cluff, L.S., and Seed, H.B. (1994) Earthquake fault rupture propagation through soil. *Journal of Geotechnical Engineering*, **120**(3), 543-561.

21. Wood, D.M. (2002) Some observations of volumetric instabilities in soils. International *Journal of Solids and Structures*, **39**(13), 3429-3449.

22. Iai, S., Tobita, T., and Nakahara, T. (2005) Generalised scaling relations for dynamic centrifuge tests. *Geotechnique*, **55**(5), 355-362.

Abbreviations

D_{50}: Soil mean grain size

E: Elasticity modulus of soil

G_s: Specific gravity

h: Fault base offset

H: Soil layer thickness

L: Soil layer length

$(\gamma_d)_{min}$ and $(\gamma_d)_{max}$: Minimum and maximum dry density of soil

v: Soil Poisson's ratio

φ_{peak}: Peak friction angle

φ_{res}: Residual friction angle

Ψ: Dilation angle

σ_v: Normal stress

Δ_y: Differential settlement at soil surface

Δ_{ys}: Rigid settlement of structure

$\Delta\alpha_1$ and $\Delta\alpha_r$: Angle between first and second story columns for the left and right column respectively

$(R.R.P)_1$ and $(R.R.P)_r$: Relative rotation percentage for the left and right column respectively

X: Displacement between right column and left side of the soil model